

Imprints of Dark Matter on Black Hole Shadows using Spherical Accretions

Saurabh^{1,*} and Kimet Jusufi^{2,3,†}

¹*Department of Physics,*

Dyal Singh College, University of Delhi-110003

²*Physics Department, State University of Tetovo, Ilinden Street nn, 1200, Tetovo, North Macedonia*

³*Institute of Physics, Faculty of Natural Sciences and Mathematics,*

Ss. Cyril and Methodius University, Arhimedova 3, 1000 Skopje, North Macedonia

We study the possibility of identifying dark matter in the galactic center from the physical properties of the electromagnetic radiation emitted from an optical-thin disk region around a static and spherically symmetric black hole. In particular, we consider two specific models for the optical-thin disk region: a gas at rest and a gas in a radial free fall. Due to the effect of dark matter on the spacetime geometry, we find that the dark matter can increase or decrease the intensity of the electromagnetic flux radiation depending on the dark matter model. To this end, we analyze two simple dark matter models having different mass functions $\mathcal{M}(r)$, with a matter mass M , thickness Δr_s along with a dark matter core radius surrounding the black hole. In addition to that, we explore the scenario of a perfect fluid dark matter surrounding the black hole. We show that in order to have significant effect of dark matter on the intensity of the electromagnetic flux radiation, a high energy density of dark matter near the black hole is needed. We also find that the surrounding dark matter distribution plays a key role on the shadow radius and the intensity of the electromagnetic flux radiation, respectively.

I. INTRODUCTION

Many modern astrophysical observatories point towards the fact that giant elliptical and spiral galaxies contain supermassive black holes (SMBHs) at their galactic centers. For example, observations suggest that at the center of our Milky Way galaxy there is a supermassive black hole with four million solar masses. These supermassive black holes are characterized by huge masses and spin parameter (or angular momenta). According to Einstein's theory of relativity, black holes generically contain a spacetime singularity at their center and an event horizon where the gravity is so strong that nothing even the electromagnetic radiation or light can escape from it. Due to the exterior spacetime geometry, black hole (BH) can capture light received from nearby stars or accretion disks into bound orbits. In other words, every black hole is characterized by the photon sphere or a collection of light rays orbiting the BH. In particular, the orbit of light is said to be unstable if the photon can fall into the BH or escape to infinity. The most compelling evidence for the existence of black holes is the first shadow images of the SMBH at the center of M87 galaxy Event Horizon Telescope (EHT) collaboration has detected [1,2] and the detection of gravity waves by LIGO [3]. It's quite amazing that we can use these precise observations to constrain different physically viable BH solutions and therefore we can test General Relativity and alternative theories of gravity, say by observing small deviations from the Kerr solution. Toward this goal, we can explore the distortion

in the shadow images which encodes valuable information about the the black hole mass/spin, and also the spacetime geometry around a given black hole solution. Furthermore, the shadow images can be used to test the existence of other exotic objects such as wormholes and naked singularities. In the literature, one can find many detailed studies concerning the black hole shadows, including static and spherically symmetric solutions, rotating solutions, and solutions in different theories of gravity [3-51]. From astrophysical point of view, it is well known that dark matter which is assumed to be some form of elementary particle it plays a key role in many astrophysical processes, yet is one of the greatest unsolved mysteries. In recent papers, the effect of dark matter on the black hole shadow has been investigated [42-51]. In this paper, we aim to study the possibility of identifying dark matter in the galactic center based on the physical properties of the electromagnetic radiation emitted from an optical-thin disk region around the static and spherically symmetric black hole. Furthermore, we shall consider a radiating optically-thin disk of gas at rest and a radiating thin disk of gas in a free fall.

The structure of our paper is laid out as follows: In Section II we point out two dark matter models; firstly we review the dark matter model proposed in Ref. [49] then we suggest a new mass function for the dark matter near the black hole. In Section III and Section IV, we study the shadow images and intensity of the radiation produced by a spherically thin medium described by a gas at rest and infalling gas model, respectively. In Section V, we study a perfect fluid dark matter model surrounding a black hole and the shadow images/intensity of the radiation produced by a gas at rest and an infalling gas model, respectively. In Section VI, we explore the connection between the shadow radius and the quasinormal modes frequencies (QNMs). Finally, in Section VII, we comment on our results.

*Electronic address: sbhkmr1999@gmail.com

†Electronic address: kimet.jusufi@unite.edu.mk (corresponding author)

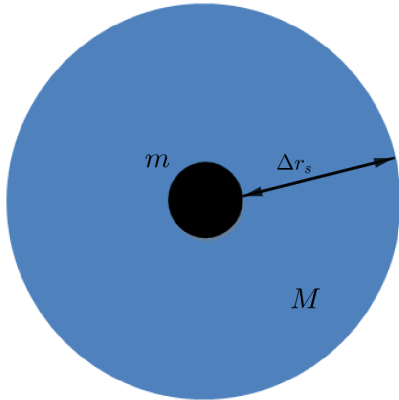


FIG. 1 A black hole with mass m surrounded by dark matter shell with thickness Δr_s and mass M . Note that $r_s = r_h$.

II. BLACK HOLE SURROUNDED BY DARK MATTER

A. Model I

Let us start by considering a toy model of a Schwarzschild black hole surrounded by dark matter proposed recently in [49]. One can then assume a piecewise function to impose three domains [49]:

$$\mathcal{M}(r) = \begin{cases} m, & r < r_s; \\ m + M\mathcal{G}(r), & r_s \leq r \leq r_s + \Delta r_s; \\ m + M, & r > r_s + \Delta r_s \end{cases} \quad (1)$$

where

$$\mathcal{G}(r) = \left(3 - 2\frac{r-r_s}{\Delta r_s}\right) \left(\frac{r-r_s}{\Delta r_s}\right)^2. \quad (2)$$

The expression for $\mathcal{G}(r)$ is chosen so that $\mathcal{M}(r)$ and $\mathcal{M}'(r)$ are continuous (see Fig. 1). The Schwarzschild metric surrounded by a spherical shell of dark matter described by Eq. (2) can be written as follows

$$ds^2 = -f(r)dt^2 + f(r)^{-1}dr^2 + r^2(d\theta^2 + \sin^2\theta d\phi^2) \quad (3)$$

in which the metric function $f(r)$ reads

$$f(r) = 1 - \frac{2\mathcal{M}(r)}{r}. \quad (4)$$

In the present work, we shall consider the nontrivial case where the dark matter is concentrated near the black hole such that $r_s = r_h$, as shown in Fig. 1. The mass function then is given by $m + M\mathcal{G}(r)$ along with $r_s \leq r \leq r_s + \Delta r_s$. From the field equations, we can compute the energy-momentum components

$$T^t_t = T^r_r = -\frac{\mathcal{M}'(r)}{4\pi r^2}, \quad (5)$$

and

$$T^\theta_\theta = T^\phi_\phi = -\frac{\mathcal{M}''(r)}{8\pi r}. \quad (6)$$

Note that we are going to consider two cases of the surrounding dark matter near the black hole; namely, a dark matter with positive energy density, i.e. when $M > 0$ (normal matter), and a dark matter with negative energy density i.e. $M < 0$. Previously, the shadow images of metric (3) and rotating counterpart of metric (3) have been studied in Refs. [49,50].

B. Model II

Here we consider another mass function choice given by the following equation

$$\mathcal{M}(r) = m + M_{DM}(r), \quad (7)$$

where the dark matter mass function is given by

$$M_{DM}(r) = \mathcal{A}r - \arctan\left(\frac{r}{\mathcal{B}}\right), \quad (8)$$

where \mathcal{A} and \mathcal{B} are constants. From the physical point of view, the constant \mathcal{B} is related to the core radius of the dark matter distribution. In what follows, we are going to investigate the possibility to detect the surrounding dark matter using the physical properties of the electromagnetic radiation emitted from an optical-thin disk region around a static and spherically symmetric black hole. As a specific example we are going to consider an optically thin and radiating gas at rest and infalling gas around a black hole.

III. OPTICALLY THIN RADIATING GAS AT REST SURROUNDING THE BLACK HOLE

Let us start by considering a general relativistic analysis for a thin radiating gas at rest in the spacetime of black hole surrounded by dark matter. To do so, we shall consider the following [27]: (i) The proper length corresponding to the coordinate interval dr is $\sqrt{1/f(r)}dr$. (ii) Every unit of energy emitted in the local frame at r corresponds to $\sqrt{f(r)}$ units of energy at infinity. (iii) A time interval dt in the local frame corresponds to an interval $dt/\sqrt{f(r)}$ at infinity. It follows that a natural choice for P_s , as well as the emission coefficient per unit solid angle j_s is the following [27]:

$$P_s(r) = \frac{1}{|g_{tt}|\sqrt{g_{rr}}4\pi r^4} = 4\pi j_s(r), \quad (9)$$

where in our case we have $g_{tt} = f(r)$ along with $g_{rr} = 1/f(r)$. The net emitted luminosity in this model, measured at infinity, reads

$$L_{emit}(r) = \int_r^\infty |g_{tt}(r')|P_s(r')4\pi r'^2\sqrt{g_{rr}(r')}dr' = \frac{1}{r}, \quad (10)$$

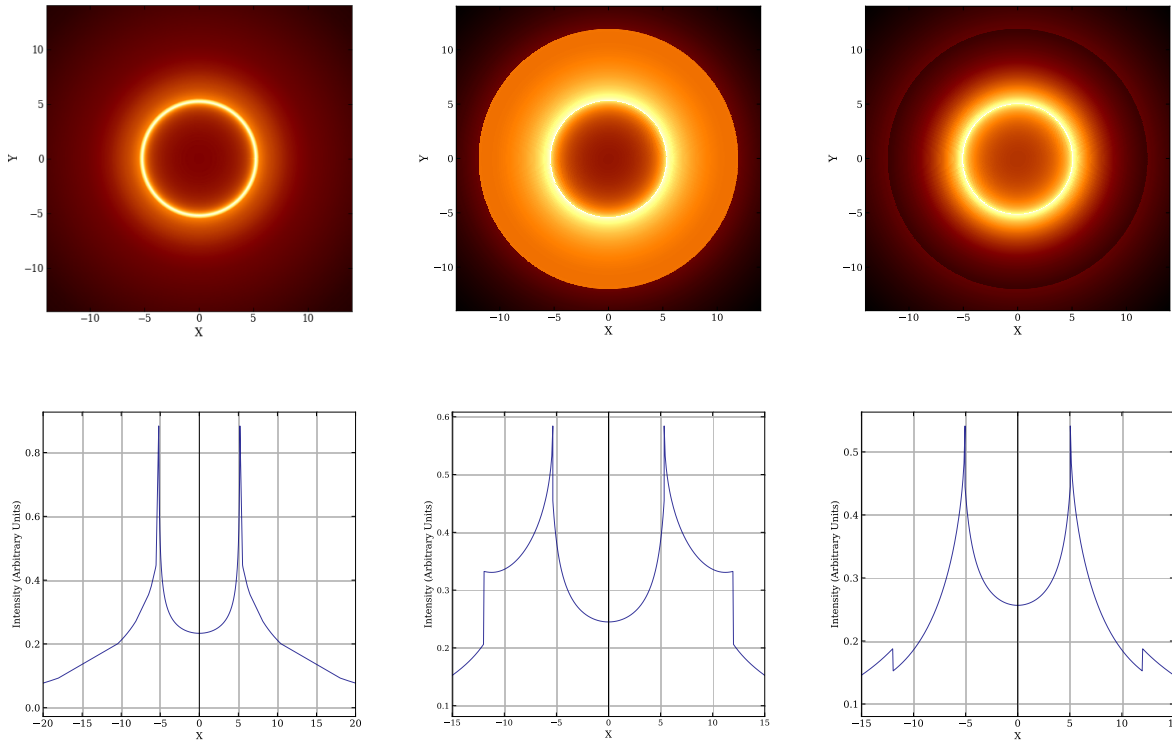


FIG. 2 From the left to the right: Image of shadows and the corresponding intensities using the rest gas model seen by a distant observer for the Schwarzschild black hole, black hole surrounded by dark matter having positive energy density $M > 0$ and negative energy density $M < 0$, respectively. We have chosen $m = 1$, $M = 1m$ along with $r_s = 2M$ and $\Delta r_s = 10M$.

which is the same result as in the Newtonian problem. However, it is interesting that only a fraction of the radiation emitted at any given r escapes to infinity and can be thus observed. It is known that the solid angle of the escaping rays is equal to $2\pi(1 + \cos\theta)$ for r outside the photon sphere radius, i.e. $r > r_{ph}$ and $2\pi(1 - \cos\theta)$ for r smaller than the photon radius, i.e. $r < r_{ph}$. Using the fact that the critical rays that barely escape have specific angular momentum equal to that of the photon orbit one can show the relation

$$\sin\theta = \frac{b}{r} \sqrt{1 - \frac{2\mathcal{M}(r)}{r}}, \quad (11)$$

where b is the impact parameter. In the case of a black hole spacetime surrounded by dark matter for the escaping rays, the net luminosity observe is found to be

$$L_\infty^{DM} = \int_{r_{ph}}^{\infty} j_s(r) 2\pi \left(1 + \sqrt{1 - \frac{b^2}{r^2} \left(1 - \frac{2\mathcal{M}(r)}{r} \right)} \right) 4\pi r^2 dr. \quad (12)$$

Using the parameters $M = m = 1$, $r_s = 2m$, and $\Delta r_s = 10M$, we find

$$L_\infty^{DM} = 0.3471235041. \quad (13)$$

In this example, the observer is located outside the dark matter halo. Consider now a more realistic situation

when the observer is located within the dark matter halo using the parameters $m = 1$, $M = 10^3 m$, $r_s = 2m$, and $\Delta r_s = 10^6 M$, and say the observer is located at $r_{obs.} = 10^3 m$. In that case, we find

$$L_\infty^{DM} = 0.335324 \quad (14)$$

We see that when the observer is located inside the dark matter halo, the net luminosity decreases. Finally, for the black hole surrounded with dark matter with $\mathcal{A} = 0.1$ along with $\mathcal{B} = 2$ and $\mathcal{B} = 10$ in the mass function (8) yields,

$$L_\infty^{DM} = 0.553555, \quad (15)$$

and

$$L_\infty^{DM} = 0.346171, \quad (16)$$

respectively. Note that for the Schwarzschild vacuum black hole we have $L_\infty = 0.3363248654$. The reduced luminosity in the latter case and the increased luminosity in the first case compared to the Schwarzschild black hole is a reflection of the fact that the gravitational deflection of light rays is bigger in the latter case while smaller in the first case. This results with a larger fraction of the emitted radiation at any r to be captured by

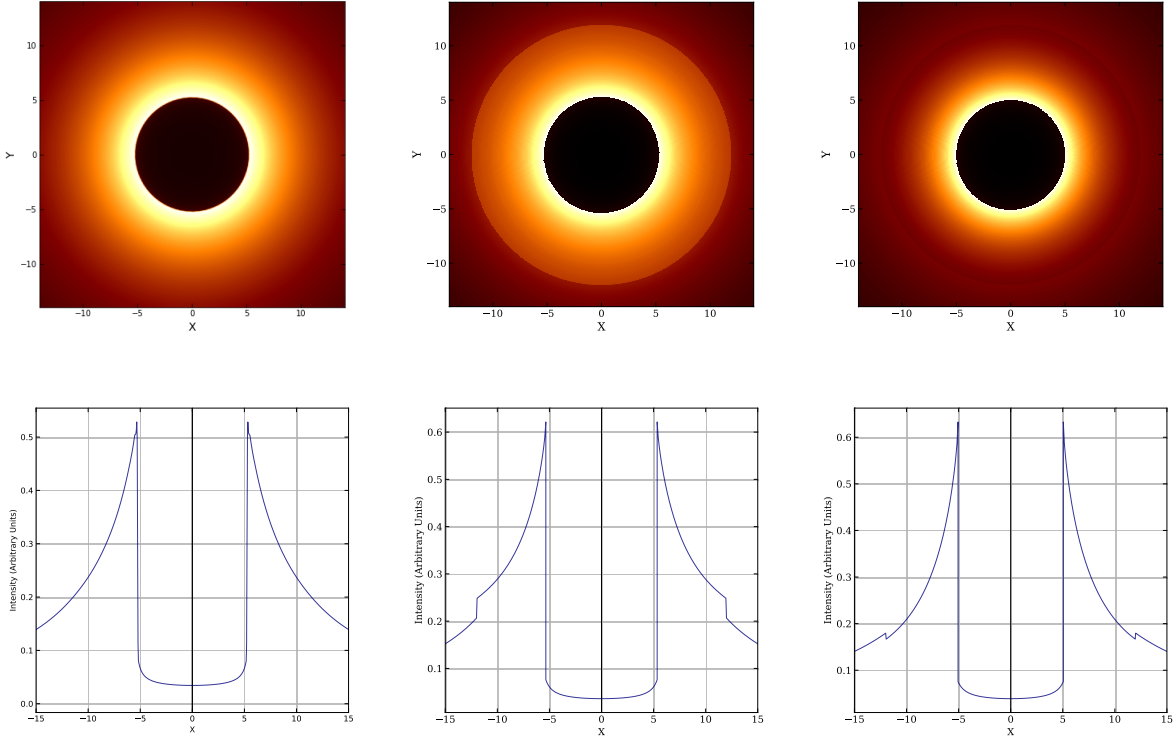


FIG. 3 From the left to the right: Image of shadows and the corresponding intensities using the infalling gas model seen by a distant observer for the Schwarzschild black hole, black hole surrounded by dark matter having positive energy density $M > 0$ and negative energy density $M < 0$, respectively. We have chosen $m = 1$, $M = 1m$ along with $r_s = 2M$ and $\Delta r_s = 10M$.

the black hole in the latter case and a smaller larger to be captured by the black hole, respectively. This shows that a high density of dark matter concentrated near the black hole implies a higher value for the the net luminosity observed at infinity. As we pointed out, this is related to the specific spacetime geometry when the dark matter is present. Next, we are interested in the image that a distant observer therefore we can use the observed specific intensity at the observed photon frequency can be found integrating the specific emissivity along the photon path

$$I_{obs}(\nu_{obs}) = \int_{\gamma} g^3 j(\nu_e) dl_{prop}, \quad (17)$$

where $g = \nu_{obs}/\nu_e$ is the redshift factor, ν_e is the photon frequency as measured in the rest-frame of the emitter, $j(\nu_e)$ is the emissivity per unit volume in the rest-frame of the emitter. The redshift factor is evaluated from $g = f(r)^{1/2}$. For the specific emissivity we assume a simple model in which the emission is monochromatic with emitter's rest frame frequency ν_* , and the emission has a $1/r^2$ radial profile:

$$j(\nu_e) \propto \frac{\delta(\nu_e - \nu_*)}{r^2}, \quad (18)$$

where δ is the Dirac delta function. The proper length can be written as

$$dl_{prop} = \sqrt{f(r)^{-1}dr^2 + r^2d\phi^2}. \quad (19)$$

It follows that the specific intensity observed by the infinite observer is

$$I_{obs}(\nu_{obs}) = \int_{\gamma} \frac{f(r)^{3/2}}{r^2} \sqrt{f(r)^{-1} + r^2\left(\frac{d\phi}{dr}\right)^2} dr \quad (20)$$

where

$$\frac{dr}{d\phi} = \pm r^2 \sqrt{\frac{1}{b^2} - \frac{f(r)}{r^2}}, \quad (21)$$

is obtained from the equation of motion obtained for the light ray that moves on the equatorial plane. In Fig. 2, we show the shadow images and the corresponding intensities using the rest gas model as seen by a distant observer for the Schwarzschild black hole surrounded by dark matter using the mass function (1). We see that having a high energy density near the black hole affects the images as well as the intensity. From Fig. 2 we see that for a given values of parameters the shadow size is decreased or increased compared to the Schwarzschild vacuum black hole. This effect in principle can be used as a tool to observe dark matter around black holes.

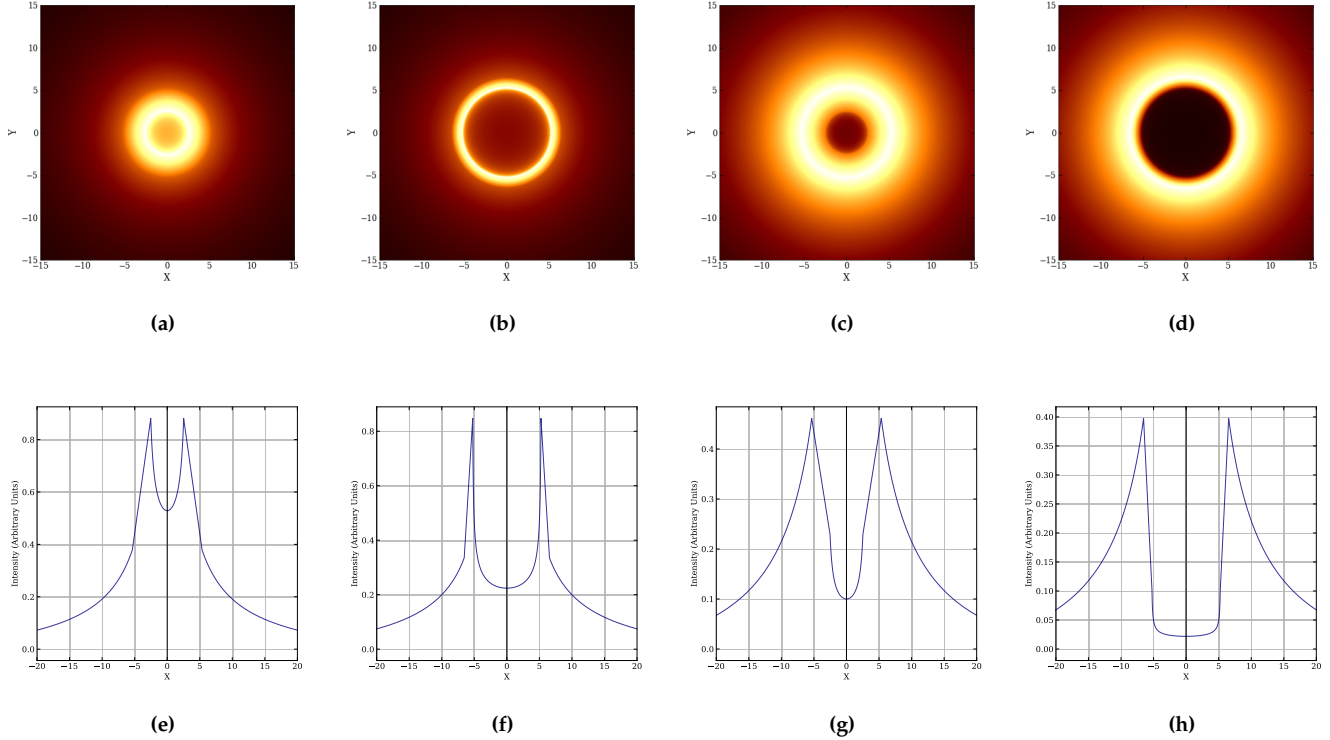


FIG. 4 From the left to the right: Images of shadows and the corresponding intensities using the rest gas model and infalling gas as seen by a distant observer in a Schwarzschild black hole spacetime surrounded by dark matter with the mass function (8). We have chosen $\mathcal{A} = 0.1$ in all plots along with $\mathcal{B} = 2$ (figures (a) and (c)) and $\mathcal{B} = 10$ (figures (b) and (d)), respectively.

IV. OPTICALLY THIN RADIATING AND INFALLING GAS SURROUNDING A BLACK HOLE

In this section we consider a more realistic model, namely an optically thin, radiating accretion flow surrounding the object and then use a numerical technique (Backward Raytracing) to find the shadow cast by the radiating flow. The calculation of the intensity map of the emitting region requires some assumption about the radiating processes and emission mechanisms. The observed specific intensity $I_{\nu 0}$ at the observed photon frequency ν_{obs} at the point (X, Y) of the observer's image (usually measured in $\text{ergs}^{-1}\text{cm}^{-2}\text{str}^{-1}\text{Hz}^{-1}$) is given by [30]

$$I_{\text{obs}}(\nu_{\text{obs}}, X, Y) = \int_{\gamma} g^3 j(\nu_e) dl_{\text{prop}}, \quad (22)$$

where $g = \nu_{\text{obs}}/\nu_e$ is the redshift factor, ν_e is the photon frequency as measured in the rest-frame of the emitter, $j(\nu_e)$ is the emissivity per unit volume in the rest-frame of the emitter, and $dl_{\text{prop}} = k_{\alpha} u_e^{\alpha}$ is the infinitesimal proper length as measured in the rest-frame of the emitter. The redshift factor is evaluated from [30]

$$g = \frac{k_{\alpha} u_{\text{obs}}^{\alpha}}{k_{\beta} u_e^{\beta}} \quad (23)$$

where k^{μ} is the four-velocity of the photons, u_e^{α} four-velocity of the accreting gas emitting the radiation, $u_{\text{obs}}^{\mu} = (1, 0, 0, 0)$ and λ is the affine parameter along the photon path γ . Here γ in the integral refers that the integral has to be evaluated along the path of the photon (null geodesics). Here we are considering a simplistic case of the accreting gas. We assume that the gas is in radial free fall with a four-velocity which in a static and spherically symmetric case reduces to

$$\begin{aligned} u_e^t &= \frac{1}{f(r)}, \\ u_e^r &= -\sqrt{\frac{g(r)}{f(r)}} (1 - f(r)), \\ u_e^{\theta} &= 0, \\ u_e^{\phi} &= 0, \end{aligned} \quad (24)$$

where

$$f(r) = g(r) = 1 - \frac{2\mathcal{M}(r)}{r}. \quad (25)$$

For the photons the four-velocity was found in the previous section. For the ease of our further calculations we find a relation between the radial and time component

of the four-velocity

$$\frac{k^r}{k^t} = \pm f(r) \sqrt{g(r) \left(\frac{1}{f(r)} - \frac{b^2}{r^2} \right)}, \quad (26)$$

where the sign $+(-)$ is when the photon approaches (goes) away from the massive object. The redshift function g is therefore given by

$$g = \frac{1}{\frac{1}{f(r)} \pm \frac{k_r}{k_t} \sqrt{\frac{g(r)}{f(r)} \left(1 - f(r) \right)}}. \quad (27)$$

For the specific emissivity we assume a simple model in which the emission is monochromatic with emitter's rest frame frequency ν_* , and the emission has a $1/r^2$ radial profile:

$$j(\nu_e) \propto \frac{\delta(\nu_e - \nu_*)}{r^2}, \quad (28)$$

where δ is the Dirac delta function. The proper length can be written as

$$dl_{\text{prop}} = k_\alpha u_e^\alpha d\lambda = -\frac{k_t}{g|k^r|} dr, \quad (29)$$

Integrating the Intensity over all the observed frequencies, we obtain the observed flux

$$F_{\text{obs}}(X, Y) \propto - \int_\gamma \frac{g^3 k_t}{r^2 k^r} dr. \quad (30)$$

In Fig. 3 we show the shadow images and the corresponding intensities using the infalling gas model as seen by a distant observer for the Schwarzschild black hole and the black hole surrounded by dark matter using the mass function (1). On the other hand, in Fig. 4 we show the shadow images and intensities for the black hole surrounded by dark matter using the mass function (8) for both gas models. Again, we observe that having a high energy density near the black hole affects the images as well as the intensity. This effect in principle can be used as a tool to observe dark matter around black holes.

1. Backward Ray tracing

Now, when we have the desired relation for the observed flux, we are ready to run our simulation. The technique that is used for making shadows of compact objects is Relativistic Ray tracing. There are two different methods with which one can do ray tracing, one of which is forward ray tracing where the light is emitted from the source, gets lensed and red/blue shifted from the object and then reach the observer's eye. Here we follow the path of the photon from the point of emission/source to the observer's eye. In terms of computing, we replace the eye with an image plane made of

pixels, so when a photon will hit one those many pixels it gets lightened up meaning that the value of pixel at that point is greater than zero. This process is repeated multiple times till the image plane filled up and is properly adjusted. Now the issue with this technique is, here we are assuming that the rays are always hitting the image plane, whereas in the real scenario the photon have a very small probability of actually hitting the eye. Potentially we would have to shoot millions and billions of rays to get only a single photon actually reaching the eye. One can argue that instead of shooting in all random directions, just shoot where the eye is. This might optimise the problem till some extent, but it is not important for the direction to be specific for diffused surfaces, which is a matter of light-matter interaction. So to sum it up this increases the computational power, which means the integration of the rays will not be that faster and is not efficient, therefore we move on to second method which is 'backward ray tracing'. Here, instead of tracing the ray from the source towards the eye, we trace the rays backwards in time, which means from the eye towards the source.

Now to implement a ray tracer the following steps were performed:

1. Shooting multiple parallel beams of light with varying impact parameters from the observer at $r_0 = 30M$ towards the object.
2. Due to a defined critical impact parameter, the rays which have $b > b_{\text{crit}}$ will get deflected and reach the source, while the ones with $b < b_{\text{crit}}$ will plunge into the the singularity.
3. Rays that gets deflected would be going from the observer towards the emitter will have some point turning point r_{tp} . So from the observer till r_{tp} the light will be red-shifted and from r_{tp} till the emitter will be blue-shifted and will illuminate the region.
4. Rays that going below the b_{crit} would be have no turning points in turn going into the singularity and having a only high red-shifted shadow, which will darken the region, hence giving out the shadow.
5. Then the corresponding intensities were plotted with respect to the impact parameter.

V. BLACK HOLE IN PERFECT FLUID DARK MATTER

We consider a $3 + 1$ gravity theory in presence of a perfect fluid dark matter (PFDM) with the action [53,54]. (see also Refs. [35, 55])

$$S = \int d^4x \sqrt{-g} \left(\frac{R}{16\pi} + \mathcal{L}_{DM} \right). \quad (31)$$

From the action we get the Einstein field equations as

$$R_{\mu\nu} + \frac{1}{2}g_{\mu\nu}R = 8\pi T_{\mu\nu}^{DM} \quad (32)$$

where $T_{\mu\nu}^{DM}$ corresponds to the energy-momentum tensor of the perfect fluid dark matter with components $(T_{\nu}^{\mu})^{DM} = \text{diag}(-\rho, P_r, P, P)$. To investigate static, spherically symmetric solutions, we employ the metric

$$ds^2 = -e^{\nu} dt^2 + e^{\lambda} dr^2 + r^2(d\theta^2 + \sin^2\theta d\phi^2), \quad (33)$$

adding the ansatz $\nu = -\lambda$, from the Einsteins field equations we find

$$e^{-\lambda} \left(\frac{1}{r^2} - \frac{\lambda'}{r} \right) - \frac{1}{r^2} = \kappa^2 T_t^t, \quad (34)$$

$$e^{-\lambda} \left(\frac{1}{r^2} + \frac{\nu'}{r} \right) - \frac{1}{r^2} = \kappa^2 T_r^r, \quad (35)$$

$$\frac{e^{-\lambda}}{2} \left(\nu'' + \frac{\nu'^2}{2} + \frac{\nu' - \lambda'}{r} - \frac{\nu'\lambda'}{2} \right) = \kappa^2 T_{\theta}^{\theta}, \quad (36)$$

$$\frac{e^{-\lambda}}{2} \left(\nu'' + \frac{\nu'^2}{2} + \frac{\nu' - \lambda'}{r} - \frac{\nu'\lambda'}{2} \right) = \kappa^2 T_{\phi}^{\phi}. \quad (37)$$

and a *prime* denotes the differentiation with respect to r . If we set $T_{\theta}^{\theta} = T_{\phi}^{\phi} = T_t^t(1 - \epsilon)$ with ϵ being a constant yielding [55]

$$\frac{P}{\rho} = \epsilon - 1. \quad (38)$$

It is interesting to note that we can find solutions that are satisfied with the condition $\lambda = -\nu$, *i.e.* $g_{tt} = -g_{rr}^{-1}$, in the limit $T_t^t \rightarrow T_r^r$. By using the equation of state for the PFDM to find the solution satisfied with the condition $\lambda = -\nu$, using $\nu = \ln(1 - U)$ with $U = U(r)$ along with the field equations it can be found [35]

$$r^2 U'' + 2\epsilon r U' + 2(\epsilon - 1)U = 0. \quad (39)$$

We can consider two special cases of the above equation.

A. Case $\epsilon = 3/2$

In this particular case it was found the following solution [35, 53]

$$U = \frac{1}{r} \left[r_s - a \ln \left(\frac{r}{|a|} \right) \right], \quad \text{for } \epsilon = \frac{3}{2}, \quad (40)$$

then the corresponding black hole spacetime in perfect fluid dark matter is given by [53, 54]

$$ds^2 = -f(r)dt^2 + \frac{dr^2}{f(r)} + r^2 \left(d\theta^2 + \sin^2\theta d\phi^2 \right), \quad (41)$$

with

$$f(r) = 1 - \frac{2m}{r} + \frac{a}{r} \ln \left(\frac{r}{|a|} \right), \quad (42)$$

where m is the black hole mass and a is a parameter describing the intensity of the dark matter. In the present work, we are going to assume $a > 0$. Hence we can write (42), far away from the black hole, as follows

$$e^{\ln \left(\frac{r}{|a|} \right)^{\frac{a}{r}}} = \left(\frac{r}{|a|} \right)^{\frac{a}{r}} \simeq 1 + \frac{a}{r} \ln \left(\frac{r}{|a|} \right) \quad (43)$$

if we identify $a \rightarrow 2v_0^2 r_0$, under this scaling we obtain in the large limit r

$$f(r) \simeq 1 + 2v_0^2(r) \ln \left(\frac{r}{2v_0^2 r_0} \right) \quad (44)$$

and the tangential velocity is a function of r , $v^2(r) = v_0^2 r_0 / r$. In order to see the physical interpretation of v_0 let us consider the isothermal dark matter density profile given by the following relation

$$\rho(r) = \frac{v_0^2}{4\pi r^2}, \quad (45)$$

along with the mass profile of the dark matter galactic halo given by

$$M_{DM}(r) = 4\pi \int_0^r \rho(r') r'^2 dr' = v_0^2 r, \quad (46)$$

can explain the flat curve of motions of stars in the galaxy. To see this, let us use the last equation to find the tangential velocity $v_{ig}^2(r) = M_{DM}(r)/r = v_0^2$ which describes a region with the nearly constant tangential speed of the stars. To do so, we can work with a static and spherically symmetric spacetime ansatz with pure dark matter in Schwarzschild coordinates the tangential velocity, one can calculate the radial function $F(r)$ by the following equation [35]

$$v_{ig}^2(r) = \frac{r}{\sqrt{F(r)}} \frac{d\sqrt{F(r)}}{dr} = r \frac{d \ln(\sqrt{F(r)})}{dr}. \quad (47)$$

Assuming a spherically symmetric solution, and solving the last equation we find

$$F(r) = \left(\frac{r}{r_0} \right)^{2v_0^2} \quad (48)$$

where r_0 is some constant. From the pure dark matter space-time it was argued that one can obtain the space-time metric of a black hole surrounded by dark matter halo solving the Einstein field equations (32) and using $T_{\mu}^{\nu DM} = \text{diag}[-\rho, p_r, p, p]$ for non-zero energy-momentum corresponding to the pure dark matter

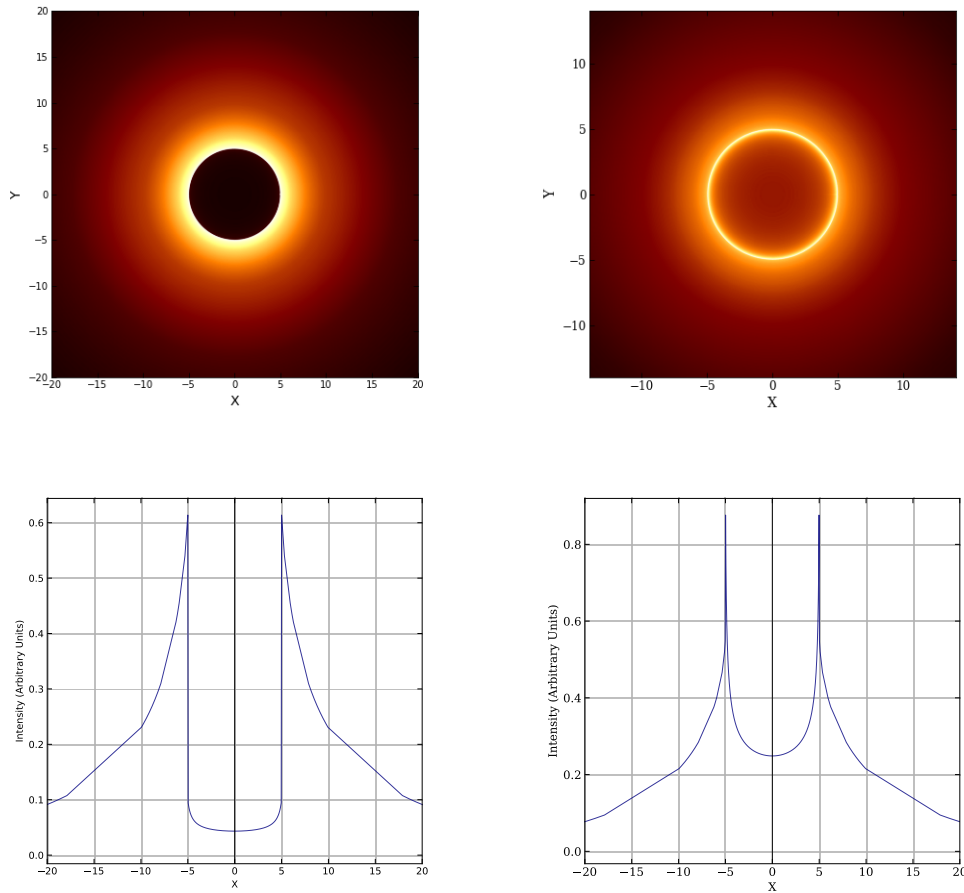


FIG. 5 Left panel: Image of shadow and the corresponding intensity using the infalling gas model in the spacetime of a black hole in perfect fluid dark matter with the metric function (56). Right panel: Image of shadow and the corresponding intensity using the rest gas model in the spacetime of a black hole in perfect fluid dark matter with the metric function (56). We have chosen $\alpha = 0.1, \gamma = 0.1, r_0 = 10^6$ in both plots.

space-time metric. One way to include the black hole in our metric is by treating the dark matter as part of the general energy-momentum tensor $T_{\mu\nu}^{DM}$. The space-time metric is chosen as (41) yielding a coefficient functions as follows (see for details [35])

$$f(r) = \left(\frac{r}{r_0}\right)^{2v_0^2} - \frac{2m}{r}. \quad (49)$$

Thus, the above space-time has a black hole in the dark matter halo. Finally, the metric coefficient $f(r)$ reduces to $f(r) \simeq 1 + 2v_0^2 \ln(r/r_0)$ which explains the flat curve of motions of stars in the galaxy having $v_0 \simeq 10^{-3}$. In other words, the last metric function describes the spacetime in the regime where the dark matter effect is not very strong and it is only a special case of the metric function (42) having constant velocity v_0 . Thus, the metric function (42) describes a strong regime of dark matter effect near the black hole. In this model, for the escaping rays, the net luminosity observed at infinity using

the parameters $m = 1$ along with $a = 1$, and $a = 2$ we find

$$L_\infty^{DM} = 0.388892, \quad (50)$$

and

$$L_\infty^{DM} = 0.416716, \quad (51)$$

respectively. If we compare now this result with the Schwarzschild vacuum solution, we see that the net luminosity observed at infinity of the black hole in perfect fluid dark matter is considerably higher. Moreover, this strong effect shows that metric function (39) describes the spacetime near the black hole surrounded by dark matter with relatively high energy density. The increase of luminosity shows that the gravitational deflection of light rays when the perfect fluid dark matter is present is considerably smaller compared to the Schwarzschild vacuum black hole. In other words, in this case, a larger fraction of the emitted radiation at any r escape from

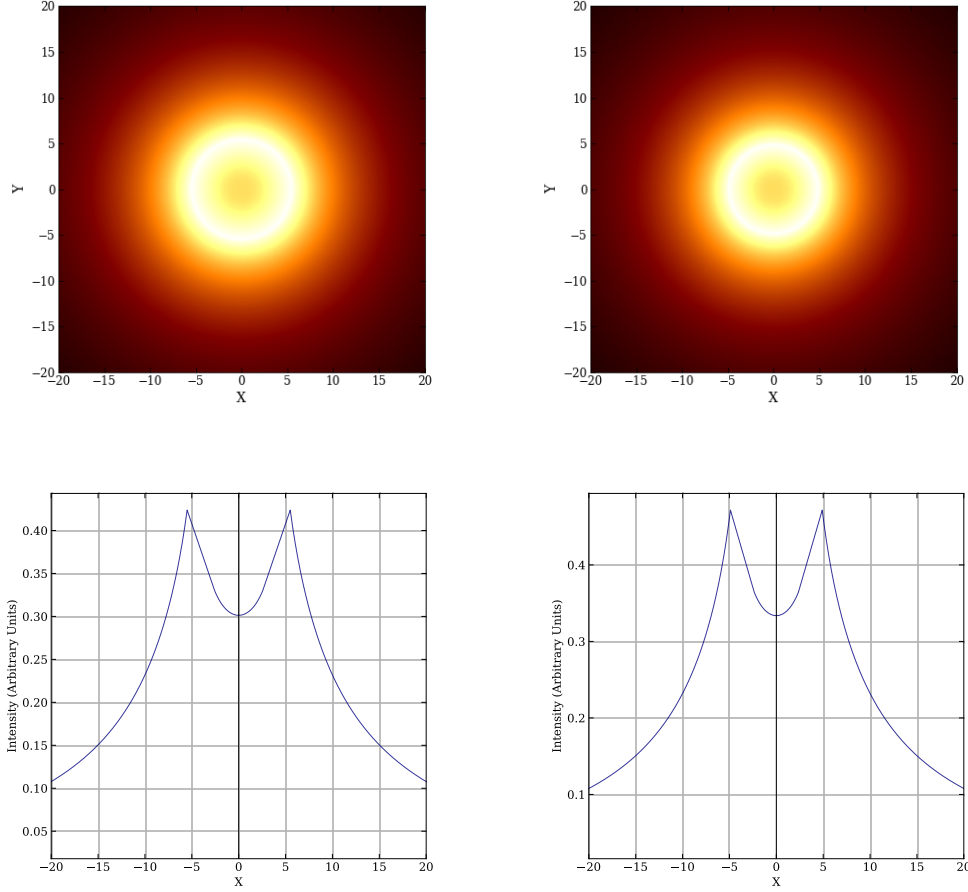


FIG. 6 Images of shadows and the corresponding intensities using the static gas model in the spacetime of a black hole in perfect fluid dark matter with the metric function (42). We have chosen for $a = 0.1$ in the left panel and $a = 0.2$ in the right panel, respectively.

the black hole as a result we observe a higher value of the net luminosity.

B. Case $\epsilon \neq \frac{3}{2}$

The solution of equation (39) in this case reads [53]

$$U = \frac{r_s}{r} - \frac{r^{2(1-\epsilon)}}{r_\epsilon}, \text{ for } \epsilon \neq \frac{3}{2}, \quad (52)$$

along with the corresponding metric given by

$$ds^2 = -f(r)dt^2 + \frac{dr^2}{f(r)} + r^2(d\theta^2 + \sin^2\theta d\phi^2), \quad (53)$$

with

$$f(r) = \left[1 - \frac{2m}{r} + \frac{r^{2(1-\epsilon)}}{r_\epsilon} \right]. \quad (54)$$

In this paper, we are interested in the metric that can describe the motions of stars in the galaxy. Therefore let us consider the scaling

$$\alpha \rightarrow 2(1-\epsilon), \quad r_\epsilon^{-1} = \gamma/r_0^\alpha, \quad (55)$$

then the metric function (53) gives

$$f = 1 - \frac{2m}{r} + \gamma \left(\frac{r}{r_0} \right)^\alpha. \quad (56)$$

This metric describes the extreme case of the dark-matter galaxy with the SMBH at its center and show the corresponding metric function $-g_{tt}$ as a function of r . Furthermore we can consider a Taylor series expansion around α far away from the black hole yielding

$$f(r) \simeq 1 + \gamma \left(1 + \alpha \ln\left(\frac{r}{r_0}\right) \right) \quad (57)$$

we see that $\gamma\alpha \simeq 2v_0^2$. In Fig. 5 we show the shadow images and the corresponding intensity using the infalling and the static gas model in the spacetime of a

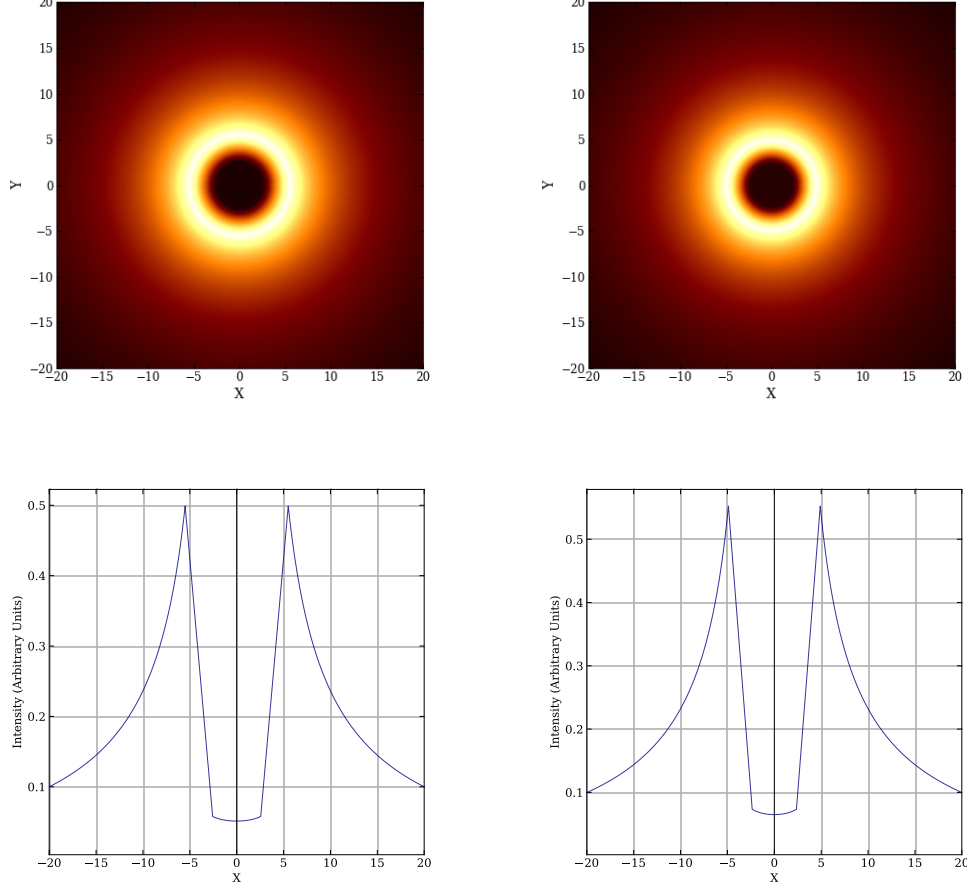


FIG. 7 Images of shadows and the corresponding intensities using the infalling gas model in the spacetime of a black hole in perfect fluid dark matter with the metric function (42). We have chosen for $a = 0.1$ in the left panel and $a = 0.2$ in the right panel, respectively.

black hole in perfect fluid dark matter described by the metric function (56). Finally in Figs. 6 and 7 we show we show the shadow images and the corresponding intensity using the static and the infalling gas model in the spacetime of a black hole in perfect fluid dark matter described by the metric function (42). We find that for a given value of parameters the surrounding dark matter can affect the intensity and the shadow radius, respectively. This shows that in principle, the shadows images of black holes with a surrounding gas at rest or infalling gas can shed some light on the problem of identifying dark matter. In a similar way, for the escaping rays, the net luminosity observed at infinity using the parameters $m = 1$ along with $\alpha = \gamma = 0.1$, and $r_0 = 10^6$ is computed to be

$$L_{\infty}^{DM} = 0.339701. \quad (58)$$

Compared to the Schwarzschild vacuum solution, we observe a very small increase in the net luminosity. This shows that the gravitational deflection angle of light in this dark matter model is slightly decreased compared

to the Schwarzschild vacuum black hole. Alternatively, we can say that the metric function (56) describes the spacetime around the black hole surrounded by dark matter with lower concentration of dark matter compared to the metric function (42) where the dark matter effect is stronger. For example, one can use (56) to explain the observed motions of stars in galaxies. On the other hand, we can decrease the core radius r_0 of the dark matter for more significant effect of dark matter, however this situation is not realistic from the astrophysical point of view where having a supermassive black hole in the center and considering the fact that the dark matter is distributed mostly in the outer part of the galaxies having r_0 of orders of few kpc.

VI. CORRESPONDENCE BETWEEN THE SHADOW RADIUS AND QNMS IN DARK MATTER SPACETIME

In this final section we precede to investigate another possible effect in the spacetime of dark matter based on

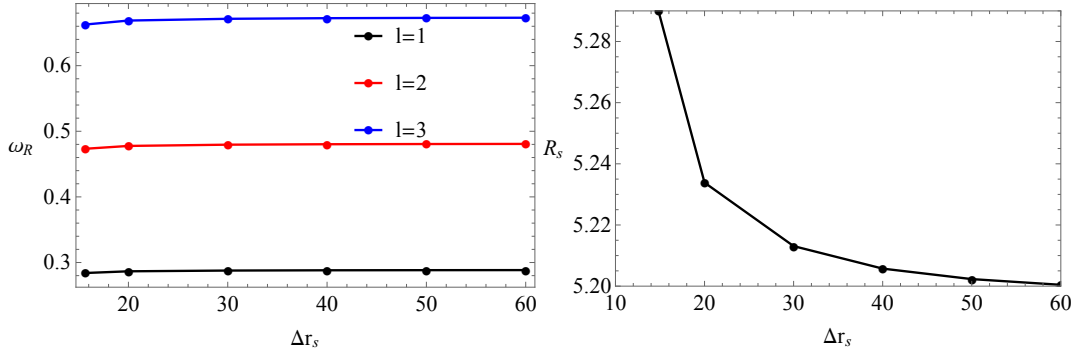


FIG. 8 QNMs frequencies obtained for the black hole surrounded by dark matter using $m = 1$, $r_s = 2m$ and positive energy density having $M = 1$.

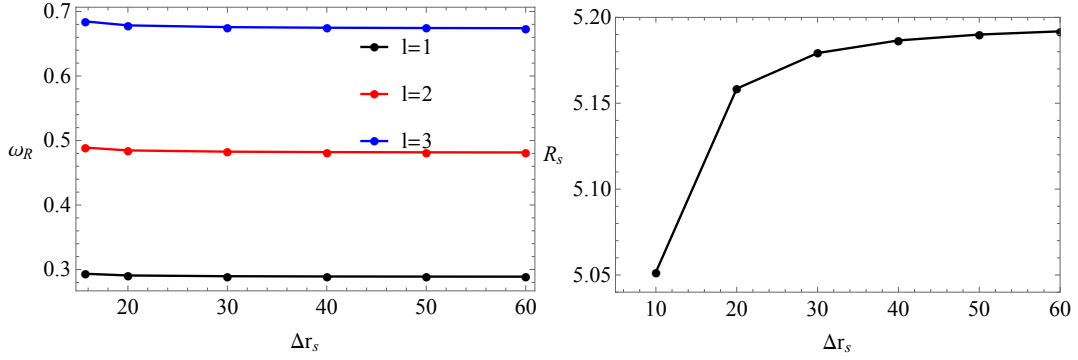


FIG. 9 QNMs frequencies obtained for the black hole surrounded by dark matter using $m = 1$, $r_s = 2m$ and negative energy density having $M = -1$.

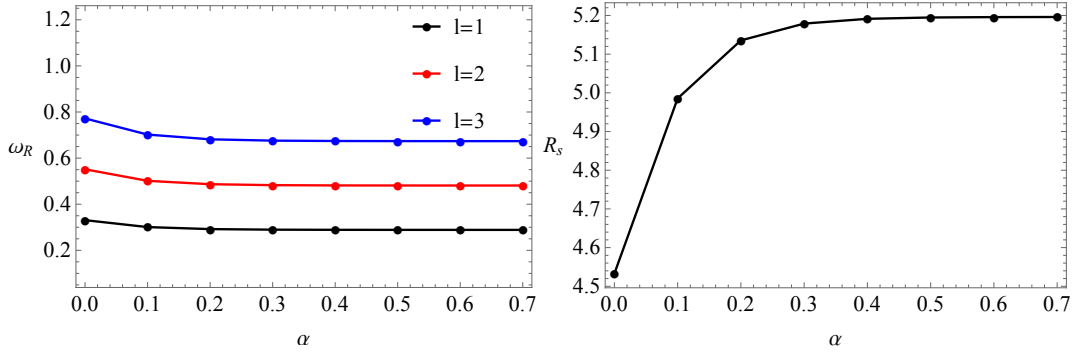


FIG. 10 Shadow radius and the real part of QNMs as a function of the parameter α . We have $r_0 = 10^6$ and $\gamma = 0.1$.

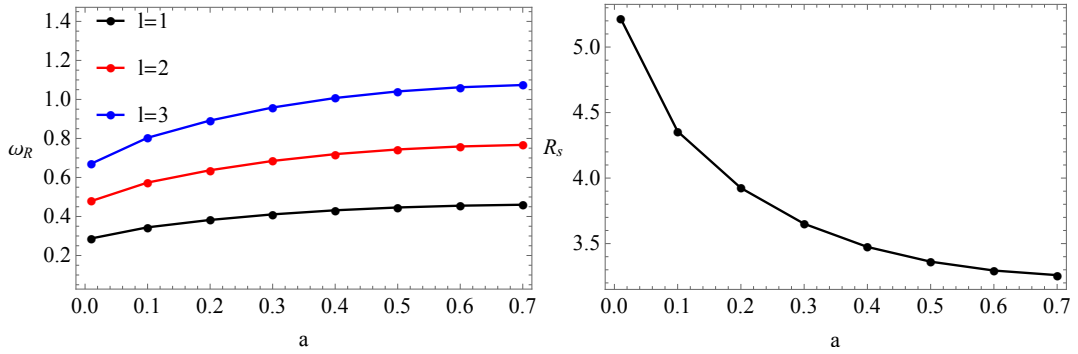


FIG. 11 Shadow radius and the real part of QNMs as a function of the parameter a .

	$l = 1$	$l = 2$	$l = 3$	$l = 4$	
$\Delta r_s [m]$	ω_{\Re}	ω_{\Re}	ω_{\Re}	ω_{\Re}	R_s
10	0.280776	0.46796	0.655144	0.842328	5.34234
10^2	0.288589	0.480982	0.673375	0.865767	5.19770
10^3	0.288674	0.481124	0.673573	0.866023	5.19617
10^6	0.288675	0.481125	0.673575	0.866025	5.19615

TABLE I Numerical values of the shadow radius and the real part of QNMs frequencies obtained for the black hole surrounded by dark matter using $m = 1$, $r_s = 2m$ and positive energy density $M = 1$.

	$l = 1$	$l = 2$	$l = 3$	$l = 4$	
$\Delta r_s [m]$	ω_{\Re}	ω_{\Re}	ω_{\Re}	ω_{\Re}	R_s
10	0.296932	0.494887	0.692842	0.890797	5.05166
10^2	0.288761	0.481269	0.673776	0.866284	5.19460
10^3	0.288676	0.481127	0.673577	0.866028	5.19614
10^6	0.288675	0.481125	0.673575	0.866025	5.19615

TABLE II Numerical values of the shadow radius and the real part of QNMs frequencies obtained for the black hole surrounded by dark matter using $m = 1$, $r_s = 2m$ and negative energy density having $M = -1$.

the field perturbations. In particular we shall investigate the correspondence between the black hole shadow in dark matter halo and the real part of QNMs frequencies. The perturbation of the black hole during the ring down phase can be studied in terms of the QNMs where one must impose an outgoing boundary condition at infinity and an ingoing boundary condition at the horizon. One can show that QNMs can be written in terms of the real part and the imaginary part representing the decaying modes

$$\omega_{QNM} = \omega_{\Re} - i\omega_{\Im}. \quad (59)$$

Previously, it has been shown that in the eikonal limit, the real part of the the QNMs frequencies mathematically are related to the angular velocity of the unstable null geodesic [7–9]. Furthermore, the imaginary part of the QNMs frequencies is linked with the Lyapunov exponent that determines the instability time scale of the orbits [7]

$$\omega_{QNM} = \Omega_c l - i \left(n + \frac{1}{2} \right) |\lambda|, \quad (60)$$

where l is the multipole number, Ω_c is the angular velocity at the unstable null geodesic, and λ denotes the Lyapunov exponent. In recent works, it was argued that the real part of the QNMs frequencies and the shadow radius, if we also include a sub-leading regime to half of its value written as are related as follows (see for details [51, 52])

$$\omega_{\Re} = R_s^{-1} \left(l + \frac{1}{2} \right), \quad (61)$$

in which R_s is the radius of the black hole shadow. This equation is accurate in the eikonal limit having large values of multipole number, i.e., $l \gg 1$. In that case we can further simplify if as $\omega_{\Re} = R_s^{-1}l$. It is thus interesting to see if we can use the above correspondence to

calculate the QNMs frequencies once we have the black hole shadow radius. As we explained, this geometric-optics correspondence becomes accurate only for large l , but sometimes works well even for the fundamental modes (compared to the scalar field perturbations). Given the fact that fundamental modes are more important from observational point of view, we present our numerical results of the real part for some fundamental QNMs frequencies presented in Tables I-III. From Table I we observe that the shadow radius decreases with the decrease of the dark matter density (increasing Δr_s). From the inverse relation between the shadow radius and the QNMs frequencies, this means that the real part of QNMs should increase with the decrease of Δr_s). In fact, we can verify this fact from the numerical values of QNMs given in Table I. In Table II, we consider the case of having dark matter with negative energy density. Quite interestingly, in this case we find that the values of the shadow radius are smaller compared to the Schwarzschild vacuum solution and increase with the decrease of energy density. The QNMs frequencies decrease with the decrease of the of energy density. This suggest that the black hole should oscillate more rapidly if we increase the amount of negative energy density of dark matter. A similar results are obtained for the perfect fluid dark matter with the metric function (42) and (56), respectively. In both cases the shadow radius is smaller compared to the Schwarzschild vacuum solution, however in the first case the shadow decreases with a and increases with α in the later case. The fact that the shadow radius is smaller compared the Schwarzschild vacuum black hole is explained from the fact that dark matter with negative energy density is involved in the perfect fluid model, provided $a > 0$ and $\alpha > 0$, respectively. For more details we refer the reader the plots of QNMs frequencies and the shadow radius shown in Figs. 8-10. Note that the fundamental modes of QNMs and the shadow radius in a static perfect fluid dark mat-

	$l = 1$	$l = 2$	$l = 3$	$l = 4$	
$a [m]$	ω_{\Re}	ω_{\Re}	ω_{\Re}	ω_{\Re}	R_s
0.1	0.334965	0.558275	0.781585	1.0049	4.35581
0.2	0.359565	0.599274	0.838984	1.07869	3.92406
0.3	0.376722	0.62787	0.879019	1.13017	3.65108
0.4	0.389437	0.649062	0.908687	1.16831	3.47439

TABLE III Numerical values of the shadow radius and the real part of QNMs frequencies obtained for the black hole surrounded by perfect fluid dark matter as a function of a .

	$l = 1$	$l = 2$	$l = 3$	$l = 4$	
α	ω_{\Re}	ω_{\Re}	ω_{\Re}	ω_{\Re}	R_s
0.1	0.300867	0.501444	0.702022	0.90260	4.98560
0.2	0.29208	0.48680	0.681521	0.876241	5.13558
0.3	0.289629	0.482715	0.675802	0.868888	5.17903
0.4	0.288943	0.481571	0.674199	0.866828	5.19134

TABLE IV Numerical values of the shadow radius and the real part of QNMs frequencies obtained for the black hole surrounded by perfect fluid dark matter as a function of α . Here we chose $\gamma = 0.1$ and $r_0 = 10^6$.

ter without accretion matter with the metric function (42) has been investigated in Ref. [51] using the WKB method. Our results in Table III, are in good agreement with the scalar field perturbations presented in [51].

VII. CONCLUSIONS

We have studied the influence of dark matter on the shadow images using the electromagnetic radiation emitted from spherical accretion medium which was assumed to be an optically-thin region surrounding the black hole. We have considered two spherical accretion models: optically-thin radiating gas at rest and a gas in a radial free fall around the static and spherically symmetric black hole. We have shown that due to the effect of dark matter on the spacetime geometry the intensity of the electromagnetic flux radiation is altered compared to the Schwarzschild vacuum black hole. In particular we have investigated two models for the dark matter distribution: Firstly, it has been analyzed the case of a total mass function which consists by a black hole with mass m , surrounded by the dark matter having mass M along with a thickness Δr_s . Secondly, we have explored the case of having a mass function given by Eq. (8). To

this end, we have considered a perfect fluid dark matter surrounding the black hole. It is found that in order to have significant effect of dark matter on the intensity of the electromagnetic flux radiation, a high energy density of dark matter near the black hole is needed. Among other things, we have shown the surrounding dark matter mass function which describes the distribution of the dark matter plays a key role on the effect of shadow images. Furthermore, we argue that if the surrounding dark matter has positive (negative) energy density the shadow radius and the intensity of the electromagnetic flux radiation increases (decreases), respectively. Finally, we have also studied the correspondence between the QNMs frequencies and the black hole shadow radius. We have shown that the shadow radius as well as the QNMs frequencies can decrease or increase depending on the concentration of dark matter near the black hole having positive or negative energy density. We should mention here that the gas medium in the present paper is optically thin accreting medium, we plan in the near future to extend our result by including a rotating accretion disk and a rotating black hole spacetime. This is of course, is outside the scope of this article.

-
- [1] K. Akiyama et al. (Event Horizon Telescope), *Astrophys. J.* **875** (2019) L1.
- [2] K. Akiyama et al. (Event Horizon Telescope), *Astrophys. J.* **875** (2019) L4.
- [3] B. P. Abbott et al. (LIGO Scientific and Virgo Collaborations), *Phys. Rev. Lett.* **116** (2016) 061102.
- [4] J. L. Synge, *Mon. Not. Roy. Astron. Soc.* **131**, no. 3, 463 (1966).
- [5] J.-P. Luminet, *Astron. Astrophys.* **75**, 228 (1979).
- [6] J. M. Bardeen, in *Black Holes (Proceedings, Ecole d'Et de Physique Thorique: Les Astres Occlus : Les Houches, France, August, 1972)* edited by C. DeWitt and B. S. DeWitt
- [7] V. Cardoso, A. S. Miranda, E. Berti, H. Witek, and V. T. Zanchin, *Phys. Rev. D* **79**, 064016 (2009)
- [8] S. W. Wei and Y. X. Liu, arXiv:1909.11911 [gr-qc].
- [9] I. Z. Stefanov, S. S. Yazadjiev and G. G. Gyulchev, *Phys. Rev. Lett.* **104** (2010) 251103
- [10] R. A. Konoplya and Z. Stuchlik, *Phys. Lett. B* **771** (2017) 597

- [11] C. Liu, T. Zhu, Q. Wu, K. Jusufi, M. Jamil, M. Azreg-Anou and A. Wang, *Phys. Rev. D* **101** (2020) no.8, 084001
- [12] X. H. Feng and H. Lu, arXiv:1911.12368 [gr-qc].
- [13] M. Zhang and M. Guo, arXiv:1909.07033 [gr-qc].
- [14] K. Hioki and K. i. Maeda, *Phys. Rev. D* **80** (2009) 024042
- [15] S.-W. Wei, Y.-X. Liu, R. B. Mann, *Phys. Rev. D* **99**, 041303 (2019).
- [16] S.-W. Wei, Y.-C. Zou, Y.-X. Liu, R. B. Mann, *JCAP* **1908**, 030 (2019).
- [17] T. Zhu, Q. Wu, M. Jamil and K. Jusufi, *Phys. Rev. D* **100** (2019) no.4, 044055.
- [18] K. Jusufi, M. Jamil, H. Chakrabarty, Q. Wu, C. Bambi, A. Wang, *Phys. Rev. D* **101**, 044035 (2020).
- [19] C. Bambi and K. Freese, *Phys. Rev. D* **79**, 043002 (2009).
- [20] C. Bambi and N. Yoshida, *Class. Quant. Grav.* **27**, 205006 (2010).
- [21] A. Abdujabbarov, M. Amir, B. Ahmedov and S. G. Ghosh, *Phys. Rev. D* **93**, no. 10, 104004 (2016).
- [22] M. Amir and S. G. Ghosh, *Phys. Rev. D* **94**, no. 2, 024054 (2016).
- [23] R. Shaikh, *Phys. Rev. D* **100** (2019) no.2, 024028.
- [24] C. Bambi, K. Freese, S. Vagnozzi and L. Visinelli, *Phys. Rev. D* **100**, no. 4, 044057 (2019).
- [25] C. Y. Chen, arXiv:2004.01440 [gr-qc].
- [26] L. Amarilla and E. F. Eiroa, *Phys. Rev. D* **85** (2012) 064019
- [27] R. Narayan, M. D. Johnson and C. F. Gammie, *Astrophys. J.* **885**, no. 2, L33 (2019)
- [28] X. X. Zeng, H. Q. Zhang and H. Zhang, [arXiv:2004.12074 [gr-qc]].
- [29] H. Falcke, F. Melia and E. Agol, *Astrophys. J. Lett.* **528** (2000), L13
- [30] C. Bambi, *Phys. Rev. D* **87** (2013), 107501
- [31] V. I. Dokuchaev and N. O. Nazarova, [arXiv:2007.14121 [astro-ph.HE]].
- [32] R. Shaikh, P. Kocherlakota, R. Narayan, P.S. Joshi, *MNRAS* **482**, 52 (2019).
- [33] G. Gyulchev, P. Nedkova, T. Vetsov and S. Yazadjiev, arXiv:1905.05273 [gr-qc].
- [34] R. Shaikh and P. S. Joshi, *JCAP* **10** (2019), 064
- [35] Z. Xu, X. Hou, X. Gong and J. Wang, *JCAP* **1809** (2018) no.09, 038
- [36] A. Allahyari, M. Khodadi, S. Vagnozzi and D. F. Mota, *JCAP* **02** (2020), 003
- [37] M. Khodadi, A. Allahyari, S. Vagnozzi and D. F. Mota, [arXiv:2005.05992 [gr-qc]].
- [38] C. Bambi, K. Freese, S. Vagnozzi and L. Visinelli, *Phys. Rev. D* **100**, no. 4, 044057 (2019) [arXiv:1904.12983 [gr-qc]].
- [39] S. Vagnozzi and L. Visinelli, *Phys. Rev. D* **100**, no. 2, 024020 (2019)
- [40] G. Gyulchev, P. Nedkova, V. Tinchev and S. Yazadjiev, *Eur. Phys. J. C* **78**, 544 (2018).
- [41] G. Gyulchev, P. Nedkova, V. Tinchev and Stoytcho Yazadjiev, *AIP Conf. Proc.* **2075**, 040005 (2019).
- [42] K. Jusufi, M. Jamil, P. Salucci, T. Zhu and S. Haroon, *Phys. Rev. D* **100**, no. 4, 044012 (2019).
- [43] S. Haroon, M. Jamil, K. Jusufi, K. Lin and R. B. Mann, *Phys. Rev. D* **99** (2019) no.4, 044015.
- [44] S.-W. Wei and Y.-X. Liu, *J. Cosmology Astropart. Phys.* **11**, 063 (2013).
- [45] Z. Xu, X. Hou and J. Wang, *J. Cosmology and Astropart. Phys.* **10**, 046 (2018).
- [46] X. Hou, Z. Xu and J. Wang, *JCAP* **12** (2018), 040
- [47] X. Hou, Z. Xu, M. Zhou and J. Wang, *JCAP* **1807**, 015 (2018).
- [48] S. Haroon, K. Jusufi and M. Jamil, *Universe* **6**, 23 (2020).
- [49] R. A. Konoplya, *Phys. Lett. B* **795** (2019), 1-6
- [50] R. C. Pantig and E. T. Rodulfo, *Chin. J. Phys.* (2020); R. C. Pantig and E. T. Rodulfo, *Chin. J. Phys.* **66** (2020), 691-702
- [51] K. Jusufi, *Phys. Rev. D* **101**, 084055 (2020)
- [52] B. Cuadros-Melgar, R. D. B. Fontana and J. de Oliveira, [arXiv:2005.09761 [gr-qc]].
- [53] M. H. Li and K. C. Yang, *Phys. Rev. D* **86**, 123015 (2012).
- [54] V.V. Kiselev (2003) arXiv:gr-qc/0303031.
- [55] Z. Xu, J. Wang and X. Hou, *Class. Quant. Grav.* **35** (2018) no.11, 115003